I Introduction

Polymer foams are of high economic and scientific interest due to their special material properties and their broad application scope [4,5]. To date, approximately 18 % of the production of the chemical industry is given by synthetic polymer materials [6] and current forecasts predict the global polymeric foam market to reach 18 MTPA by 2015 [7]. Particularly in the field of thermal insulation materials the application of polymer foams has been gaining more and more importance since the last years and decades [8]. Apart from the rising energy prices, one main cause for this increase can be found in official regulations for building insulations, that have been tightened in recent years [9-13]. The European Energy Efficiency Directive for example, that was approved in 2012, intends to reduce the energy consumption in the EU by 20 % until 2020 [14]. This implies incisive measures for the enhancement of the energy efficiency of buildings [1] as more than a quarter of the energy consumption is accounted for by private households, which use almost three quarters of the energy for space heating/cooling [15,16]. Therefore, especially insulation materials have to be improved constantly.

In the vast numbers of different polymeric materials polymethylmethacrylate (PMMA) and polystyrene (PS) are two prominent polymers. Although the two polymers have several commonalities, the areas of application differ decisively. Whereas PS foams are mainly used for building insulation, PMMA is marked by its durability, a high level of optical transparency and an exceptionally good resistance to weathering [17]. Therefore, it is mainly designated to be used in civil engineering, automotive industry and aeronautics [18]. PMMA foams which combine optical transparency with outstanding insulation properties are not yet available, but exhibit a huge market potential. In order to realize such a high-potential material, the pore size of PMMA foams has to be reduced to submicron range. On the one hand, the scattering of light is expected to be negligible when the pore size is much smaller than the wavelength of visible light, so that PMMA nanofoams would be optical transparent. In addition, the thermal heat conductivity is considerably reduced by taking advantage of the so called *Knudsen* effect. When the pore size of a foam is smaller than the mean free path length of the enclosed gas [19-21], the heat transfer of the cell gas collapses as can be seen by plotting the gaseous thermal conductivity as function of the pore size (Fig. 1-1). The mean free path length of air (black line in Fig. 1-1) at room temperature and atmospheric pressure is approximately $\lambda_{air} \approx 70$ nm [22].

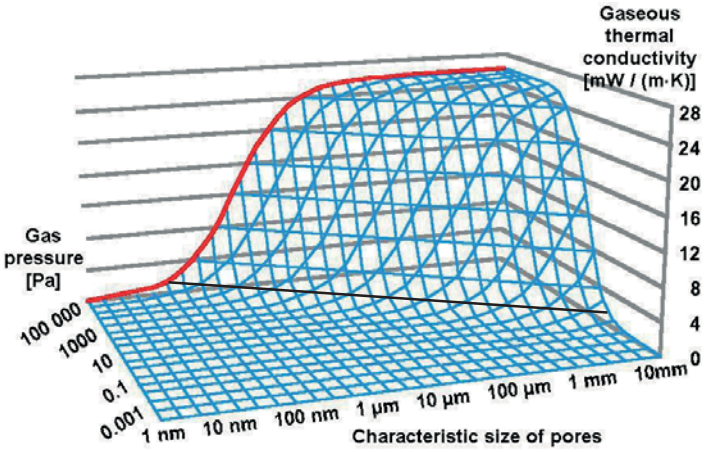

Fig. 1-1: Calculated values for the gaseous thermal conductivity of air-filled pores in a polymer foam as function of the characteristic pore size and pressure (taken from [23]). The mean free path length of air as function of the pressure (black solid line) was added to the plot for a better classification.

As a matter of course, this relation is also valid for PS foams. In contrast to PMMA, polystyrene-based foams, like EPS® or XPS®, already have a broad application in building insulation [17,24]. Consequently, there is a high economic and ecological interest in a further improvement of existing polystyrene insulation wall panels.

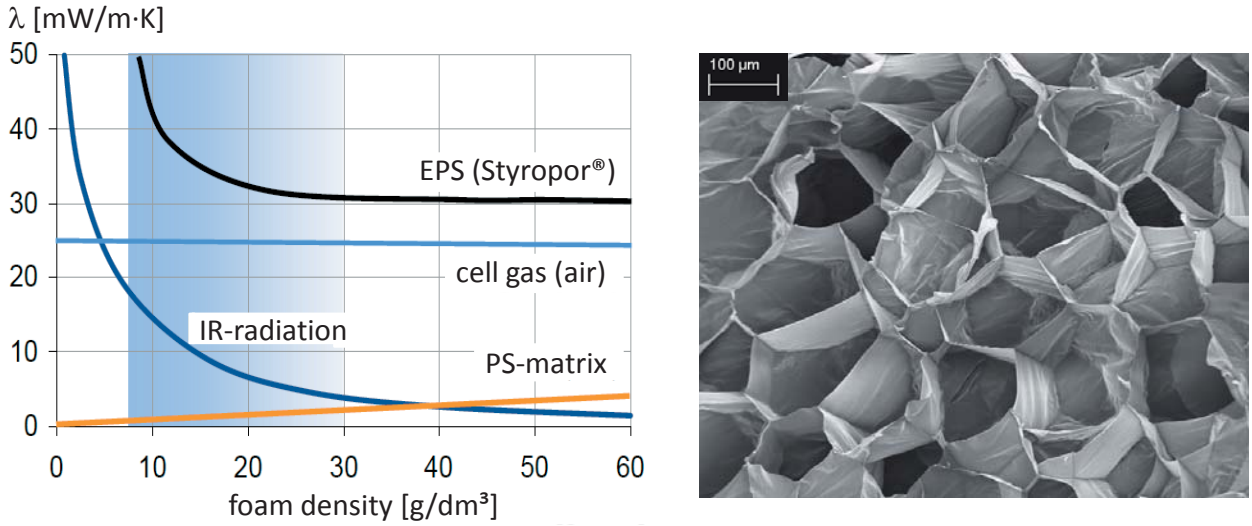

Fig. 1-2, *left*: Plot of the different contributions to the total thermal conductivity (λ) as function of the foam density for Styropor® (taken from [25]). *Right*: Scanning electron microscopy image of Styropor®.

For a commercially available polystyrene foam (Styropor®, see Fig. 1-2) with pore sizes in the range of 100 µm and foam densities of 30 to 50 g/dm^3 the predominant contribution to the overall thermal conductivity is caused by the enclosed cell gas ($\lambda_{cellgas} \approx 25$ mW/m·K), while the heat transmission originating from infrared radiation and the PS matrix is of comparatively little relevance ($\lambda_{matrix} + \lambda_{radiation} \leq 10$ mW/m·K). Under consideration of the above-mentioned *Knudsen* effect, illustrated in Fig. 1-1, λ-values as low as 10 mW/m·K are realizable if the pore size is reduced sufficiently. This significant reduction of thermal

conductivity would entail significant material savings and enable a thinning of the wall panels at constant insulation properties. Particularly in consideration of the fact that the average thickness of polystyrene insulation panels has been increased from 7.2 cm to 12.5 cm in the last 15 years [8], the remarkable market potential becomes apparent. Furthermore, the volume reduction would facilitate the waste disposal as the low density and the statutory need for a thermal recycling [26] cause additional logistic costs and transport emissions [27]. Apart from an improvement of the insulation properties and the accompanying benefits, nanofoams would feature a higher mechanical stability that would result in an extension of the damage-free life period. This in turn would prolong the usage time after amortization for end-users. Consequently, an application of PS nanofoams as insulation material would reduce not only direct but also indirect energy consumption. *Jelle et al*. come to a similar evaluation as they predict nano insulation materials (NIMs) to be the most suitable insulation materials of the future [1].

Without any doubt, the same level of economization through pore size reduction is applicable to PMMA nanofoams leading to a total thermal conductivity as low as about 15 mW/m·K in consideration of the slightly higher heat transfer of the PMMA matrix (λ_{PMMA} = 190 mW/m·K [28]) compared to PS (λ_{PS} = 170 mW/m·K [29]). This very low λ–value in combination with optical transparency would enable an expansion of existing and a creation of new PMMA-markets.

The current production of foamed polymeric materials is either based on foaming techniques, in which chemical as well as physical blowing agents are applied, or on template strategies. Foaming processes that make use of chemical blowing agents are characterized by the utilization of a chemical reaction, in which gas is released simultaneously to the polymerization. A prominent example for such a process is the production of polyurethane foams [30-32]. The use of physical blowing agents usually refers to an extrusion process, which implies a saturation of a molten thermoplastic polymer with a propellant (nowadays mostly *n*-pentane or CO_2) [33-39]. The subsequent expansion leads to a nucleation of the blowing agent and therefore to the formation of foam pores within the polymer matrix. Foams thus obtained show a typical pore size of 100 µm.

In order to reduce the pore size *Colton* and *Suh* developed a two-step technique in 1987 that starts with a saturation of polystyrene based polymers with an inert blowing agent [40-44]. Afterwards the polymer is brought above its glass transition temperature (T_G) by

heating before the pressure is released. This creates the intended porosity in the thermoplastic material and leads to foams with pore sizes below 10 µm. Transferring this approach to polymers with a much higher T_G like polyetherimides *Krause et al.* were the first to prepare thermoplastic material with an open cell porosity below 100 nm, which they termed nanofoams [45-49]. Nevertheless, these two step techniques are only applicable to very thin films of a few millimeters to ensure a sufficient gas saturation of the polymer, which already takes hours. As such they are inappropriate for the production of nanoporous bulk materials.

As already mentioned also template-strategies are used for the production of nanoporous materials in different approaches. This technique utilizes a mixture of at least two components which is structured at micro- or nanoscale. If one of the components is fixed selectively, the other components can be removed by resolving or extraction leaving a replica of the previous structure behind. Using concentrated oil-in-water macroemulsions as template enables the synthesis of highly porous bulk material, inorganic and organic, when the aqueous component is fixed by polymerization [50-56]. Since large amounts of oil are undesirable from an environmental point of view and additionally, the removal of the oil has to be performed very carefully in order to preserve the template structure, *Cooper et al.* used CO_2 instead of oil. This yielded in an almost one to one conversion of the template structure into a fixed material in which the pore sizes are again in the range of 10 µm [57-61]. It is obvious that the minimal pore size obtained by the template strategy is given by the domain size of the template. Thus, for macroemulsions resulting structural sizes in the range of several microns are to be expected.

To date, aerogels are the only commercially available nanoporous bulk materials. The network of these highly porous solids can consist of organic, inorganic and organic-inorganic hybrid joints depending on the chemical composition of the starting material [62-68]. But in all cases aerogels are synthesized via the sol-gel process invented by *Kistler* [69-71]. In this process a condensable substance is solved in an adequate solvent before a catalyst is added that induces a formation of sol particles with sizes of only a few nanometers. In the further course of the process these particles aggregate to a network that builds the frame of the later aerogel. In order to remove the solvent, supercritical fluids are used to avoid a destruction of the framework. The structure of the aggregated sol-template is at least two orders of magnitude smaller than the emulsion template. Consequently, the interfacial area between both components and therefore the total

interfacial energy of the system is much higher making the removal of the solvent even more crucial. The supercritical drying in turn has the benefits of a slow and steady change of the fluid density and therefore of the interfacial tension between the solid material and the fluid when the pressure is reduced carefully. Because of this time consuming and critical drying step, aerogels are expensive and their application is limited to special fields like space engineering [72,73].

Due to their thermodynamic stability and self-organization at nanoscale, microemulsions are promising template systems for the production of nanoporous materials. They consist at least of one hydrophilic and one hydrophobic component that are separated by an amphiphilic (surfactant) layer. The drastic reduction of interfacial tension, that is caused by the surfactant, enables the thermodynamic stability [74-77]. Various attempts have been carried out to solidify the dynamic microstructure of microemulsions by polymerization [78-95]. However, the production of highly porous materials failed, due to the sensitivity of appropriate microemulsion templates. An enhancement of this microemulsion template strategy is given by the "Principle of Supercritical Microemulsion Expansion" (POSME) procedure that was invented by *Strey*, *Sottmann* and *Schwan* in 2003 [2,96]. This principle is based on the substitution of the liquid oil component by a supercritical (*sc*)fluid leading to an expandable microemulsion template (for a detailed description of the POSME procedure see section 2.1.3). The expansion of the *sc*fluid swollen micelles allows a drastic increase of volume before, while or after polymerization, which enables the preparation of highly porous materials. Additionally, the density reduction of the propellant occurs steadily and without a nucleation step as the fluid being in a supercritical state.

Of course, the formulation of the *sc*-microemulsion is the essential step for the POSME procedure. In this context the oil substitute of choice is CO_2, because it is inflammable, non-toxic, bio-/food-compatible and inexpensive. That is why the phase behavior as well as the microstructure of *sc*CO_2-in-water microemulsions has been systematically elucidated by *Schwan* [97], *Kramer* [98] and *Klostermann* [99] in the last few years. These investigations were based on prior studies in which microemulsions containing ethane and propane as well as water-in-*sc*CO_2 microemulsions were examined [100-112]. But the solidification of the nanostructure is challenging, because polymerizations usually cause a change in composition that leads to demixing processes of the sensitive microemulsion [79-81]. Within the POSME procedure additionally the polymerization process has to be timed precisely. A premature fixation would prevent a foaming process, whereas the foam

would coarsen dramatically when not fixed directly after expansion. *Klostermann* was able to avoid this difficulty expanding propane swollen micelles in a highly concentrated sugar solution. Here, the fixation of the homogeneous phase occurs during expansion due to the fact that the glass transition of the sugar solutions is crossed [99,113]. In this way sugar foams that feature pore sizes of only a few microns could be obtained.

In general, the expansion is the most critical step in foaming processes. Although the structure of the starting material and the resulting foam are usually well understood, the structural changes occurring during expansion are nearly uninvestigated for various reasons. On the one hand, foaming processes are usually very fast and irreversible, which complicates the application of indirect analyzing methods like scattering experiments. On the other hand, if structural dimensions at nanoscale are desired, the foaming process occurs also at nanoscale so that optical investigations are almost impossible. Nevertheless, a possibility to get a detailed insight into the occurring processes during the early state of foaming, is given by the utilization of the POSME procedure. This is enabled by the fact that the (pressure induced) segregation of microemulsions is reversible to a certain extent. Hence, the process can be repeated as many times as necessary by performing pressure cycles until scattering data with sufficient statistics to characterize each state is collected. Because of a characteristic length scale in the range of a few nanometers [114], time resolved small angle neutron scattering (SANS) experiments are best suited for the examination of pressure induced phase separations in microemulsions as representative model for foaming processes.

At the outset of this work no experimental scattering setup existed that allowed to carry out periodic pressure cycles. In this context the Stroboscopic High Pressure SANS cell (SHP-SANS cell, section 2.2.2) had to be developed and improved. A second problem that had to be tackled was the time resolution of neutron scattering experiments, which is always limited by the wavelength distribution of neutrons. In order to overcome this restriction it was planned to integrate the "Time Involved Small Angle Neutron Experiments option (TISANE-option [115,116], section 2.2.4)" into the experimental setup of the D22 at the ILL (Grenoble, France) within the framework of a BMBF-project [117].

Beyond the early foaming state studies by means of the POSME procedure, the effectiveness of so called "Anti Aging Agents" (AAA) can be investigated by the same measuring technique. The application of AAA in foaming processes was invented by *Strey et al.* in order to suppress aging phenomena, like *Ostwald* ripening [118] or

coagulation with subsequent coalescence [119] that cause a coarsening of the foam structure. An AAA can be any low molecular hydrophobic substance that is homogeneously dissolved in the blowing agent above a certain pressure. The approach is based on the fact that if the pressure is dropped below the critical pressure of the mixture at critical composition of blowing agent and AAA, the low molecular oil wets the expanding interface. Comparing the interfacial tensions of the gas-liquid and liquid-liquid interface [120] an AAA is expected to have a decelerating effect on aging phenomena occurring during the foaming process. Thus, more time is available to solidify the template nanostructure.

Evidentially, the POSME procedure cannot be used to produce polymeric foams out of hydrophobic monomers (like PMMA and PS). Therefore, another approach for the production of PMMA and PS nanofoams was employed in this thesis that enables the formation of propellant droplet number densities in the same order of magnitude (about 10^{16} - 10^{17} droplets per cubic centimeter). This new approach is called "Nano-Foams by Continuity Inversion of Dispersion" (NF-CID) and was submitted as patent application by *Strey* and *Müller* in 2011 [3]. The NF-CID procedure utilizes nanodisperse voids in dense amorphous or crystalline packings of colloidal polymer nano-latices. These voids are filled with a super- or near-critical fluid at appropriate pressures and at temperatures below but close to the glass transitions temperature of the respective polymer. This filling is completed within a few seconds, because of the enormous surface area of the colloidal crystal and the smaller fluid-polymer interfacial tension compared to the air-polymer interfacial tension. When T_G is traversed a "continuity inversion" can be observed, the formerly discrete polymer particles are turning into a continuous polymeric material with nanodisperse inclusions of the supercritical fluid. Here, the diameter and the number density of the inclusions are directly proportional to the size of the particles. A subsequent expansion leads to a foaming process with a fixation of the polymer foam when temperature and/or pressure dropped (a detailed explanation of the NF-CID procedure is given in section 3.1). Note, that the NF-CID procedure is not restricted to polymer-fluid systems that are miscible to a certain extent, as the nanodisperse propellant pools are generated by the continuity inversion instead of fluid-saturation of the polymer.

Because of the simple nature of the NF-CID procedure, it is not limited to PMMA, PS or polymers at all. Rather all thermoplastic materials that can be provided in form of nanoparticles can theoretically be converted into nanofoams, opening a broad field of possibilities for the production of innovative materials.

OBJECTIVES

Since there are two main goals, namely the elucidation of foaming processes by means of kinetic SANS studies in combination with the POSME procedure and the synthesis of polymeric nanofoams via the NF-CID principle, this work is divided into two parts.

In order to formulate CO_2-microemulsions, fluorinated surfactants have proven to be most effective [104,108,109,121-125]. Therefore, a water-rich CO_2-microemulsion of the type water - CO_2 - technical grade polyethyleneglycol- perfluoroalkylether was planned to be chosen as basic system. But meaningful investigations of the kinetics can only be conducted if the static properties of the CO_2-microemulsion are well understood. Consequently, first the phase behavior and the microstructure had to be characterized at different oil mass fractions and temperatures. Then pressure induced changes of the microstructure (in the range from p = 300 bar to 150 bar) were to be studied using time-resolved small angle neutron scattering in combination with the newly designed SHP-SANS cell that provides adjustable pressure cycles.

Based on the obtained results first pressure jumps into the two-phase region (in the range from p = 150 bar to 70 bar) were to be performed and characterized by time-resolved SANS measurements. As microemulsions containing a gas or a fluid as oil component are templates for nanofoams these investigations can be seen as a representative model system for the early state in foaming processes. Additionally, the influence of cyclohexane, used as AAA, on the microstructure and on the kinetics was planned to be studied for validating the slowing down of aging phenomena during the foaming process. Moreover, the addition of cyclohexane enables the application of film contrast conditions as the deuteration degree of water can be matched to the mixture of CO_2 and cyclohexane-d12.

In the second part of this work the NF-CID principle should be applied in order to produce PMMA and PS nanofoams. In this context the main focus was on the influence of the different foaming parameters on the resulting foam. The main foaming parameters are the diameter of the particles in the colloidal crystal, the foaming temperature, the exposure time as well as the CO_2 pressure. All foams thus obtained were to be characterized by means of scanning electron microscopy (SEM) and the pore sizes should be considered in relation to theoretical values. In parallel, the transferability of the NF-CID principle to a pilot plant scale was to be examined using PMMA.

2 CO_2-Microemulsions as Template for Nanofoams: Kinetic SANS-Studies

2.1 Water-rich Microemulsions

In general microemulsions are defined as thermodynamically stable and nanostructured mixtures of at least three components [74-76]. While two components, a polar and a nonpolar, are almost immiscible, the third component, a surfactant, enables a mixing of the polar and nonpolar phase. A surfactant is an amphiphilic molecule that is therefore miscible with both polar and nonpolar phases, and if both phases are present they are separated by a surfactant monolayer. This results in a drastic reduction of the interfacial tension and in a thermodynamically stable state. Although microemulsions are macroscopically homogeneous and isotropic mixtures, a variety of morphologies can be found at microscopic scale. Depending on composition, temperature and pressure spherical and cylindrical micelles or inverse micelles as well as bicontinuous networks and liquid crystalline phases can be obtained in the one-phase region [75,126-128]. Beside this one-phase region there are also two- and three-phase regions depending again on temperature, composition and pressure.

In 1943 *Schulman* was the first to find macroscopically homogeneous mixtures that gleam bluish [77,129]. He named these mixtures microemulsions. A first characterization of microemulsions was performed by *Winsor* in 1954 who studied the three phase region by using ionic surfactants [130]. The influence of the temperature and of the amount of a nonionic surfactant was then investigated by *Shinoda* and *Friberg* in 1981 [131,132]. Finally the work of *Kahlweit* and *Strey* led to a fundamental understanding of phase behavior and microemulsions [74,133-135].

2.1.1 Phase Behavior

The best way of getting an understanding of the complex phase behavior of microemulsions is to first have a look at the three binary mixtures shown in Fig. 2-1. The binary phase diagram of water (A) and oil (B) is representative for the ordinary situation that those components are nearly immiscible, i.e. the miscibility gap can be found over the whole temperature range and the upper critical point lies far above the boiling point. Looking at the phase diagram of oil (B) and nonionic surfactant (C) it becomes obvious that there is only a lower miscibility gap with an upper critical point cp_α. The corresponding critical temperature T_α is strongly dependent on the nature of surfactant and oil and can be found below as well as above the freezing point of the mixture [134]. Because of having both a lower miscibility gap and a closed upper miscibility gap the phase diagram of water (A) and surfactant (C) is the most complex. Usually the lower miscibility gap lies far below the freezing point of the mixture. That is why it will be neglected in further discussions. In contrast the upper miscibility gap and the lower critical point cp_β are highly relevant for the theoretical description of microemulsions. The lower critical temperature T_β is in the relevant region and depends again on the used surfactant while the upper critical temperature of this gap is usually above the boiling point. Studying the microstructure of this mixture it was found that at intermediate temperatures the surfactant is dissolved as monomers at low surfactant concentrations until the critical micelle concentration (cmc) is reached where the surfactant starts to aggregate and form micelles [136]. If the surfactant concentration is increased further even liquid crystalline phases can be found [137].

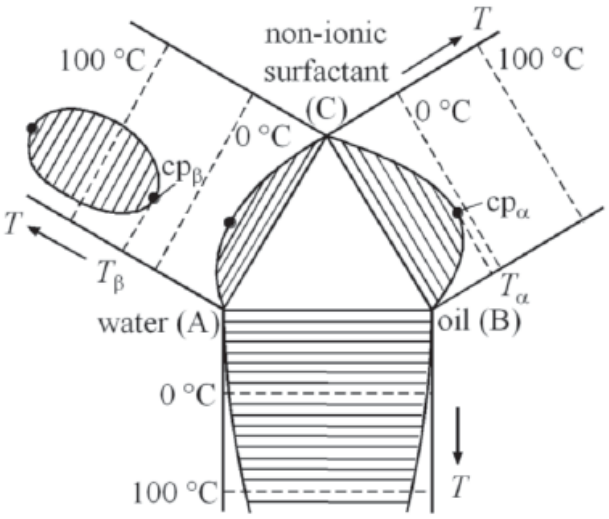

Fig. 2-1: Schematic drawing of the three binary systems of water (A), oil (B) and nonionic surfactant (C). Together they build the basis for the phase prism of a ternary mixture [74].

If the binary systems are combined and flipped up a phase prism of the ternary system water (A) - oil (B) - nonionic surfactant (C) is received (*Gibbs* triangle, Fig. 2-2). The temperature dependent phase behavior is ruled by the interaction of the upper miscibility gap in the A-C-mixture and the lower miscibility gap in the B-C-mixture. In other words, the phase behavior is determined by the change of solubility of the surfactant in water and oil when the temperature is varied. This change of solubility has its origin in the partial dehydration of the surfactant head groups that occurs at higher temperatures [138].

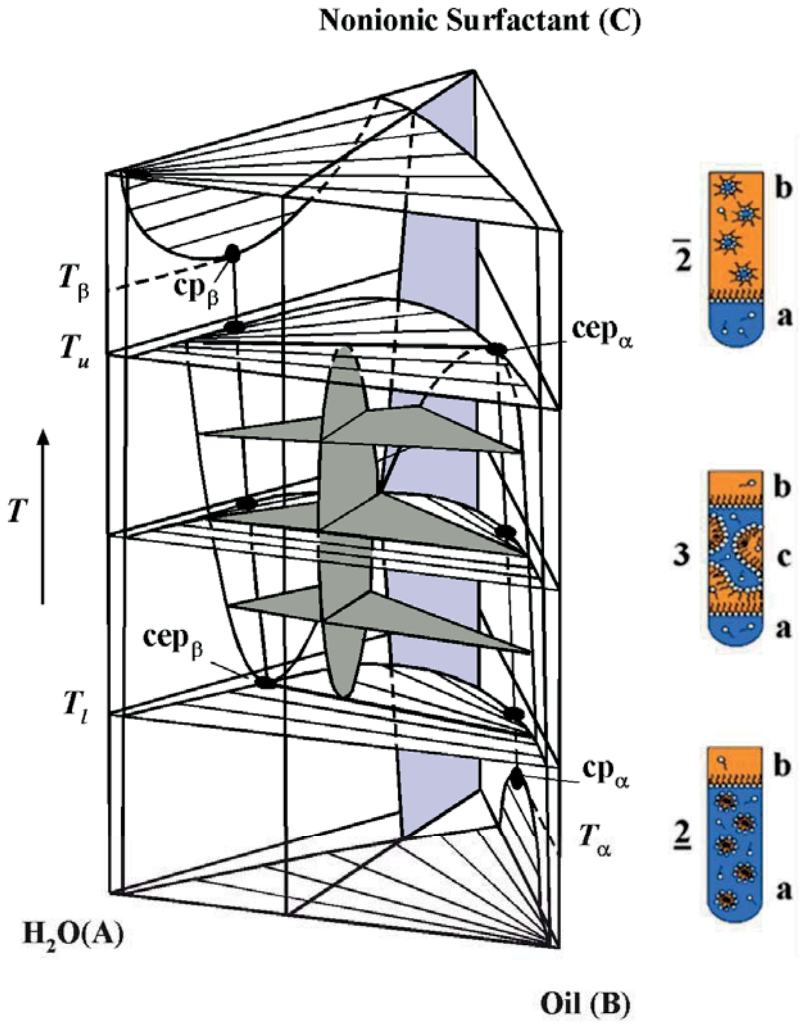

Fig. 2-2: Schematic drawing of a phase prism of the ternary system water - oil - nonionic surfactant (*Gibbs* triangle). The temperature dependent phase behavior for all possible compositions of the three components becomes obvious by combining and flipping up the three binary systems. The section that is drawn in by a constant water to oil ratio is the so called $T(\gamma)$–section. Here, the one-phase region is colored in blue while the three phase region is marked in grey. By means of the test tubes on the right hand side the phase inversion in this $T(\gamma)$–section is illustrated [139].

Starting at temperatures higher than T_u, a water-in-oil (w/o)-microemulsion (b) can be found in coexistence with a water excess phase (a) shown in the upper test tube. Because of

the water having usually a higher density than the oil rich microemulsion and because of the dash signalizing the location of the surfactant rich phase, this state is called $\bar{2}$. The slope of the tie-lines in the *Gibbs* triangle at T_u indicates the composition of the excess phase. When the temperature is now decreased the surfactant head groups become more and more hydrated so that the water solubility increases. As a consequence, below T_u a three phase region (3) is formed, in which the surfactant and oil rich middle phase (c) coexist with an oil (b) as well as a water (a) excess phase (represented by the middle test tube). By lowering the temperature further the phase c changes at $T = (T_u+T_l)/2$, where an equal composition can be found, from an oil rich to a water rich microemulsion until T_l is crossed and again a two-phase region is formed ($\underline{2}$). In contrast to the two-phase region at higher temperatures here the surfactant rich phase is an oil-in-water (o/w)-microemulsion that coexists with an oil excess phase as shown in the lower test tube. Again, this can be explained by the temperature dependent water solubility of the surfactant. This sequence ($\bar{2}\rightarrow 3\rightarrow \underline{2}$) from $T > T_u$ to $T < T_l$ is called phase inversion.

OIL-IN-WATER MICROEMULSIONS

For characterizing such microemulsion systems there are different possible sections that can be performed through the phase prism [76]. Beside the common $T(\gamma)$–section (water to oil ratio is kept constant) that is drawn in Fig. 2-2, with which the minimal amount of surfactant $\tilde{\gamma}$ that is necessary to solubilize a certain water to oil ratio can be determined, also sections are performed in which the water to surfactant ratio is kept constant and small amounts of oil are added ($T(w_B)$-section). In this case the maximum amount of oil that can be solubilized by a certain water-surfactant mixture can be determined. These systems show nearly the same temperature dependent sequence of different phases as already mentioned for $T(\gamma)$–sections. Starting at low temperatures again a $\underline{2}$-region can be found. Depending on the amount of oil added a three or a one-phase region can be found when temperature is increased. In the case of a $T(w_B)$-section the lower phase boundary can be found at or below T_l. This phase boundary is called oil emulsification failure boundary (*oefb*) [140,141]. A further increase of temperature leads to the formation of a $\bar{2}$-region. In contrast to the $T(\gamma)$–section the phase boundary between the one-phase region and the $\bar{2}$-region is more complex because of having a minimum. In order to describe the

origin of this minimum the single *Gibbs* phase triangles have to be taken into account. They are shown together with the corresponding $T(w_B)$-section in Fig. 2-3.

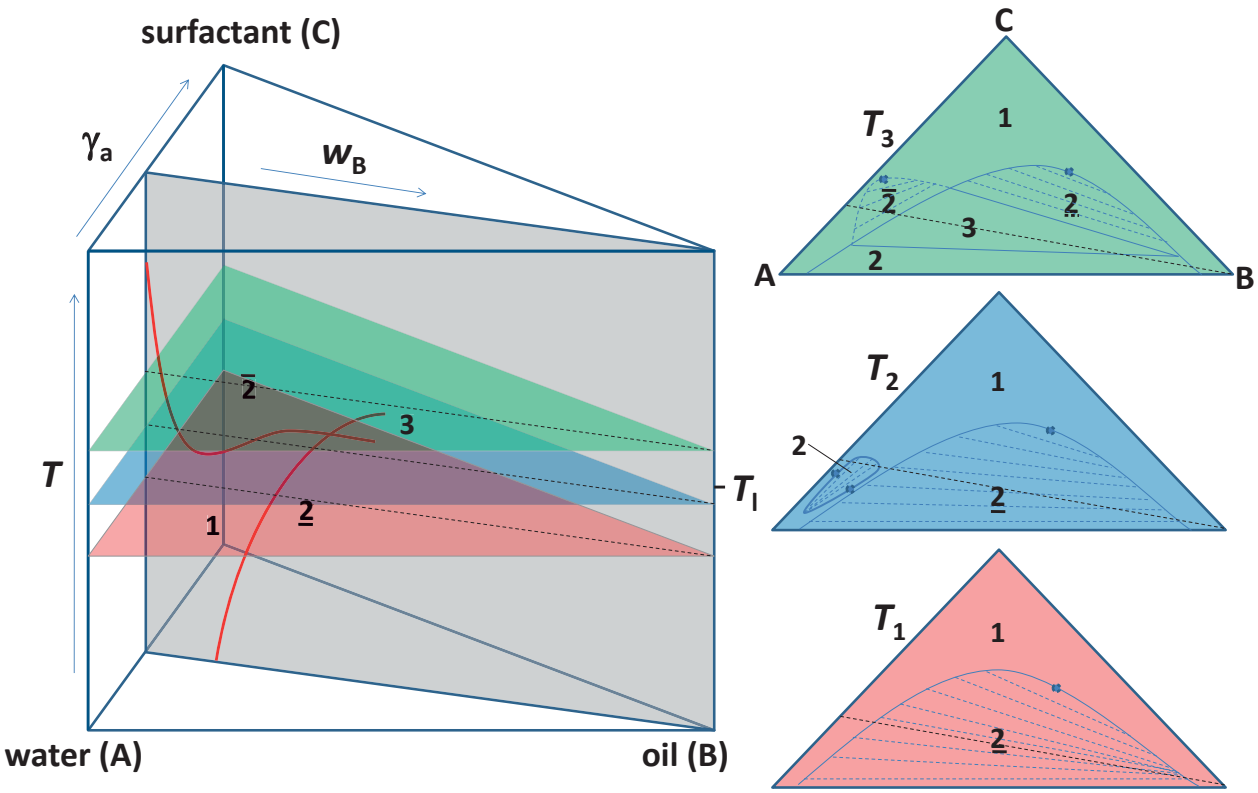

Fig. 2-3, *left*: Section through the phase prism at a constant water to surfactant ratio γ_a. The phase boundaries are determined by varying the overall oil weight fraction w_B and the temperature. *Right*: *Gibbs* phase triangles at a certain temperature. The lines represent the phase boundaries while the blue dashed lines are the critical tie-lines and the dots the corresponding critical points. Especially the blue colored triangle in which the closed loop is shown on the left hand side is important for the description of the minimum in the upper phase boundary.

By considering the isothermal sections (*Gibbs* phase triangles) shown in Fig. 2-3 (right) the origin of the *oefb* and the upper phase boundary become obvious. At the lowest displayed temperature T_1 the one-phase region is in coexistence with the $\underline{2}$-region. The dot at the upper right side of the phase boundary represents the critical point at this temperature and the blue dashed lines are the corresponding tie-lines. With the help of these tie-lines the composition of each point within the $\underline{2}$-region can be determined by the lever rule. Therefore, the negative slope indicates that a surfactant rich water phase is in coexistence with an oil excess phase as it is always the case in the $\underline{2}$-region. Looking at the temperature T_2 that is close beneath T_I two alterations can be noticed. On the one hand, the critical point has shifted a little bit to the left so that the slope of the tie-lines has become less steep. However, the more important change is, on the other hand, that a two-phase region arises

at the left hand side. This region with two critical points is the so called closed loop and it is the reason for the upper phase boundary running through a minimum. The origin of this closed loop will be discussed in detail in the section 2.1.2. However, the characteristic of the closed loop and therefore the minimum in the upper phase boundary depends on the chain length of the surfactant [142]. For short chain (weak) surfactants, like C_6E_3, the upper phase boundary descends monotonically to T_l while long chain surfactants, e.g. $C_{12}E_5$, show the discussed minimum as well as a clearly higher efficiency (compare Fig. 2-4). This is a result of the better interaction between the surfactant and the oil. Finally, the *Gibbs* triangle at T_3 in Fig. 2-3 that is slightly higher than T_l has to be considered. At this temperature the one-phase region can only be found at a very small w_B. With an increasing amount of oil a $\bar{2}$-region is passed, in which the tie-lines show a positive slope, i.e. the microemulsion phase is in coexistence with a water excess phase until a three phase region is reached.

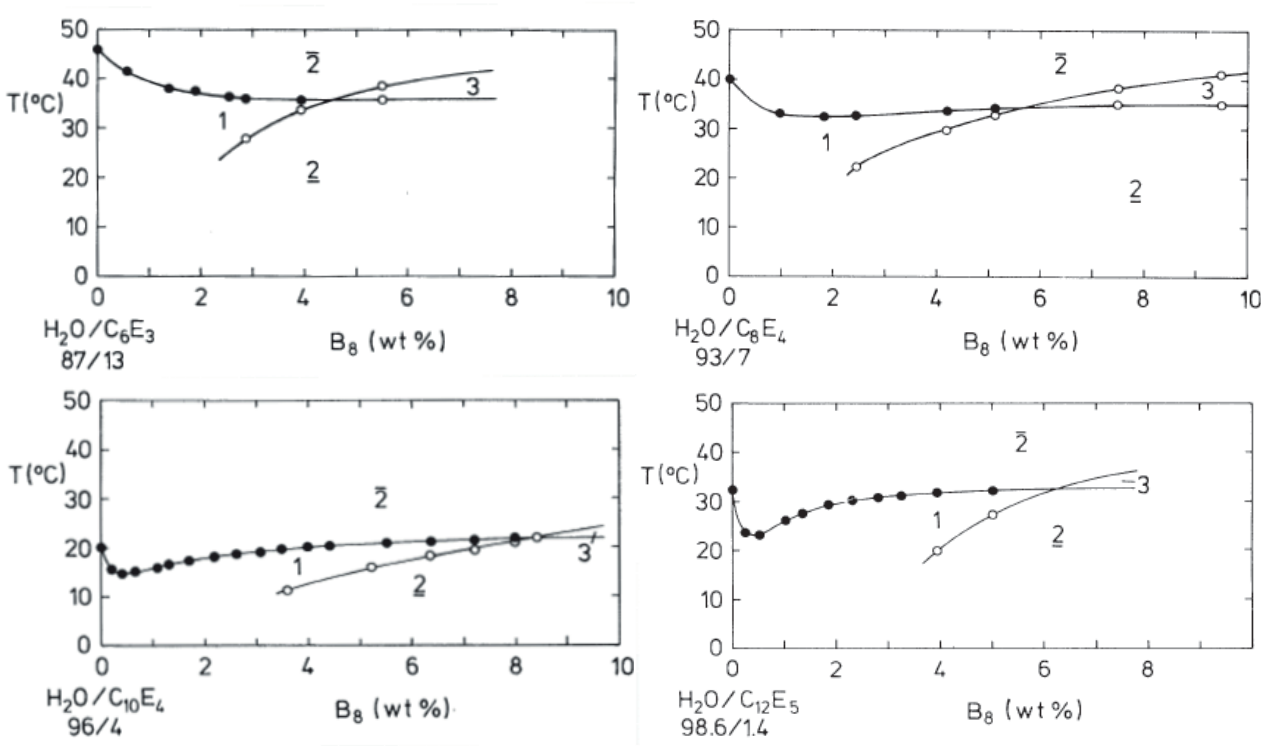

Fig. 2-4: $T(w_B)$-sections (here w_B is denoted as B_8) for different nonionic surfactants of the system water - octane - C_iE_j (taken from [142]). The higher *i* and *j* are, the more oil can be solubilized in the water-surfactant mixture (Note, that the amount of surfactant γ_a is decreased for higher *i* and *j*). This is a result of the higher amphiphilicity of the surfactant and the associated better interaction between the hydrophobic chain of the surfactant and oil. Additionally, the discussed minimum of the upper phase boundary appears when using $C_{10}E_4$ and becomes even more pronounced for $C_{12}E_5$. Again, this can be related to the better structuring properties of the surfactant.

DEFINITION OF USED PARAMETERS

For the specification of water-rich microemulsions it is common to define mass fractions that allow a complete description of the composition. The water-surfactant mixture is described by the parameter γ_a that is given by

$$\gamma_a = \frac{m_{\text{surfactant}}}{m_{\text{water}} + m_{\text{surfactant}}} \qquad \text{Eq. 2-1}$$

and the amount of oil in the mixture is specified by w_B:

$$w_B = \frac{m_{\text{oil}}}{m_{\text{water}} + m_{\text{oil}} + m_{\text{surfactant}}} . \qquad \text{Eq. 2-2}$$

Although the ratios of water, oil and surfactant can be described with the help of Eq. 2-1 and Eq. 2-2 sufficiently, the composition of each phase itself has to be defined, too. Therefore the parameter ψ that gives the mass fraction of an additive to the water phase

$$\psi = \frac{m_{\text{water -additive}}}{m_{\text{water -additive}} + m_{\text{water}}} \qquad \text{Eq. 2-3}$$

and the parameter β that gives the mass fraction of an additive to the oil phase

$$\beta = \frac{m_{\text{co-oil}}}{m_{\text{co-oil}} + m_{\text{oil}}} \qquad \text{Eq. 2-4}$$

have to be taken into account.

Additionally, if a salt is added to the aqueous phase the mass fraction ε is defined by

$$\varepsilon = \frac{m_{\text{salt}}}{m_{\text{salt}} + m_{\text{water}}} . \qquad \text{Eq. 2-5}$$

Finally the parameter δ is needed, which defines the composition of the surfactant phase if more than one surfactant is used:

$$\delta_{\text{surfactant}} = \frac{m_{\text{surfactant}}}{m_{\text{surfactant}} + m_{\text{co-surfactant}}} , \qquad \text{Eq. 2-6}$$

where *n* is the number of used surfactants.

The above-mentioned parameters will always be related to H_2O throughout this work if D_2O or a H_2O/D_2O mixture is used for SANS experiments.